Experimental Neurology 388 (2025) 115226

Contents lists available at ScienceDirect

Experimental Neurology

journal homepage: www.elsevier.com/locate/yexnr

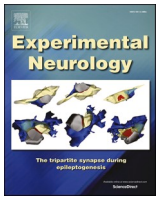

Research paper

Lack of effects of Resolvin D1 after spinal cord injury in mice

Isaac Francos-Quijorna [a,1], Néstor López-González [a], Marc Caro-Canton [a], Alba Sánchez-Fernández [a], Gerard Hernández-Mir [b], Rubèn López-Vales [a,*]

[a] Departament de Biologia Cel·lular, Fisiologia i Immunologia, Institut de Neurociències, Centro de Investigación Biomédica en Red sobre Enfermedades Neurodegenerativas (CIBERNED), Universitat Autònoma de Barcelona, Bellaterra, 08193, Catalonia, Spain
[b] Centre for Immunobiology, Blizard Institute, Barts and The London School of Medicine, Queen Mary University of London, London E1 2AT, UK

ARTICLE INFO

Keywords:
Resolvin D1
Maresin 1
Inflammation
Inflammatory resolution
Neuroprotection
Spinal cord injury
MicroArray

ABSTRACT

Inflammation is a fundamental component of the body's response to injury or infection and is responsible for restoring tissue homeostasis and starting the wound healing process. To avoid excessive tissue damage, it is important to efficiently resolve inflammation once it is no longer necessary. In recent years, the discovery of pro-resolving lipid mediators derived from polyunsaturated fatty acids, such as Resolvin D1 (RvD1), has shed light on the resolution of inflammation. However, the impact of RvD1 on Spinal Cord Injury (SCI) remains unexplored. In this study, we provide direct evidence that the administration of RvD1 for one week after SCI fails to enhance resolution of inflammation and does not improve functional and histological outcomes. Our transcriptomic analysis reveals that RvD1 does not modulate inflammatory response pathways in the injured spinal cord but leads to significant changes in the expression of genes related to ribosomal function and extracellular matrix pathways. Unlike SCI, RvD1 treatment ameliorated neurological deficits in experimental autoimmune encephalomyelitis. Our findings represent the first report demonstrating that RvD1 treatment does not exert therapeutic actions in the context of SCI and suggest that this pro-resolving agonist may exert therapeutic actions in certain but not in all conditions involving an inflammatory component.

1. Introduction

Traumatic SCI results in permanent disability due to irreversible axonal damage and neuronal and glial death. The initial mechanical injury is followed by a range of cellular and molecular events, referred to as the secondary injury phase. During this phase, the initial damage expands to regions surrounding the lesion core, exacerbating cell death, axonal disruption, and functional impairments (Oyinbo, 2011). Inflammation plays a crucial role in triggering secondary tissue damage after SCI. Although the inflammatory response is critical in the acute phase for restoring tissue homeostasis and initiating wound repair, improper continuing effects of this physiological mechanism after SCI leads to excessive tissue damage (Buckley et al., 2014; Serhan, 2014; Serhan et al., 2015).

We previously revealed that, in line with post-mortem brain samples from Alzheimer's disease patients (AD) (Wang et al., 2015; Zhu et al., 2016), there is defective production of Specialized Pro-resolving Mediators (SPMs) after SCI, which it is associated with inadequate resolution of inflammation (Francos-Quijorna et al., 2017). In this study, we also demonstrated that administration of Maresin-1 (MaR1), a docosahexaenoic acid (DHA)-derived SPM, facilitates the resolution of inflammation and leads to therapeutic benefits. Thus establishing a critical link between the absence/low levels of SPMs in the injured spinal cord and the consequential hindrance in resolving inflammation and mitigating tissue damage. In line with these observations, we also found a similar relationship in experimental autoimmune encephalomyelitis (EAE), a mouse model of multiple sclerosis (Sanchez-Fernandez et al., 2022). While our results shed light on the beneficial effects of MaR1, the exploration of other DHA-derived SPMs, such as RvD1, remains to be thoroughly investigated.

RvD1 (7S,8R,17S-trihydroxy-4Z,9E,11E,13Z,15E,19Z-DHA) is a biologically active molecule synthesized from DHA by the action of 15- and 5-lipoxygenases (LOX) (Hong et al., 2003). RvD1 exerts its effects by binding to the G protein-coupled receptors (GPCR), GPR32 and ALX/

* Corresponding author at: Facultat de Medicina, Universitat Autònoma de Barcelona, 08193 Bellaterra, Spain.
E-mail address: Ruben.Lopez@uab.cat (R. López-Vales).
[1] Present address: Immunometabolism and inflammation laboratory, Centro de Biología Molecular Severo Ochoa (CBMSO), Consejo Superior de Investigaciones Científicas (CSIC)-Universidad Autónoma de Madrid (UAM), 28,049 Madrid, Spain

https://doi.org/10.1016/j.expneurol.2025.115226
Received 24 December 2024; Received in revised form 9 March 2025; Accepted 19 March 2025
Available online 20 March 2025

FPR2 (Bisicchia et al., 2018; Chiurchiù et al., 2016; Chiurchiù et al., 2019; Gilligan et al., 2019; Krishnamoorthy et al., 2010), which are expressed in various endothelial, immune, and neural cells. The pro-resolution properties of RvD1 are mediated by limiting leukocyte infiltration, suppressing the production of pro-inflammatory cytokines, switching immune and epithelial cells from a pro-inflammatory to an anti-inflammatory state, and enhancing the clearance of immune cells from the challenged tissues (Chiurchiù et al., 2016; Chiurchiù et al., 2019; Hoch et al., 2023; Krishnamoorthy et al., 2010; Norling et al., 2012b; Pope et al., 2016; Recchiuti et al., 2011; Rogerio et al., 2012; Titos et al., 2011). In the context of neurological conditions, RvD1 has been shown to exert neuroprotective effects. Previous studies revealed that this SPM reduces neuroinflammation and improves cognition in AD (Fiala et al., 2016; Mizwicki et al., 2013; Pope et al., 2016) and mitigates the progression of EAE (Poisson et al., 2015) through various mechanisms, including the induction of Treg cells and the polarization of monocytes/macrophages and microglia into the anti-inflammatory M2-like phenotype. Furthermore, in the context of central nervous system (CNS) injury, RvD1 treatment has been shown to reduce the activation of microglial cells and astrocytes after remote brain damage, thereby preventing neuronal cell death (Zhang et al., 2018). Despite these promising pro-resolutory actions of RvD1 in the CNS, to the best of our knowledge, no studies have assessed the therapeutic potential of RvD1 in SCI.

The current study aims at evaluating the efficacy of exogenous delivery of RvD1 in mitigating inflammation and secondary damage after SCI in mice. Contrary to MaR1 (Francos-Quijorna et al., 2017), we found that RvD1 administration failed to improve resolution of inflammation and to confer protection against tissue damage and functional impairments after SCI.

2. Materials and methods

All the experimental procedures were approved by the Universitat Autònoma de Barcelona Animal Experimentation Ethical Committee (CEEAH 4053 M-) and followed the European Communities Council Directive 2010/63/EU, and the methods for each procedure were carried out in accordance with the approved guidelines.

2.1. Surgical procedure

Adult (8–10 weeks old) female C57Bl/6 mice (Charles River) were deeply anesthetized with intramuscular injection of a mixture of ketamine (90 mg/kg) and xylazine (10 mg/kg). After performing a laminectomy at the 11th thoracic vertebrae, the exposed spinal cord was contused using the Infinite Horizon Impactor device (Precision Scientific Instrumentation) (Francos-Quijorna et al., 2017; Klopstein et al., 2012). Injuries were made using a force of 60 kdynes and tissue displacement ranging between 400 and 600 μm (Coll-Miró et al., 2016; Francos-Quijorna et al., 2017).

2.2. RvD1 treatment after SCI

One hour after SCI, mice received an intravenous injection of either 0.5, 1, or 2 μg of RvD1 (7S,8R,17S-trihydroxy-4Z,9E,11E,13Z,15E,19Z-docosahexaenoic acid; Cayman Chemical Company, Ann Arbor, MI) followed by daily injections until day 7 ($n = 3$ per dose). These doses were based on previous studies in the literature using SPMs in neurological conditions (Francos-Quijorna et al., 2017). Additionally, another larger cohort of mice received 1 μg of RvD1 daily for seven days ($n = 7$ per group)), beginning 1 h after injury ($n = 8$ in vehicle and $n = 10$ in RvD1) or on day 1 post-injury (n = 7 per group). The RvD1 solution was freshly prepared from stock on the day of administration. Each preparation consisted of 10 μl of 100 % ethanol containing the specified amount of lipid mediator, diluted in 100 μl of saline at 37 °C. The solution was individually prepared in Eppendorf tubes (one per mouse) and injected within 15 min of preparation. Control mice were treated with the vehicle solution, which consisted of 10 μl of 100 % ethanol diluted in 100 μl of saline at 37 °C, following the same administration protocol.

2.3. Cytokine protein expression

Mice treated with vehicle or RvD1 ($n = 5$ per group) were perfused with sterile saline and a 5 mm length of spinal cord centered on the lesion was collected at 12 h after contusion injury and snap frozen. Spinal cords were homogenized, and protein concentration was determined using the DC Protein Assay (Bio-Rad). Samples were concentrated to 4 μg/μl using MicroCon centrifugation filters (Millipore) to ensure equal amounts of protein. The protein levels of 20 cytokines and chemokines were then analyzed using the Milliplex MAP Mouse Cytokine/Chemokine magnetic bead panel (Millipore) on a Luminex (Millipore) as per manufacturers' protocol (Coll-Miró et al., 2016; Francos-Quijorna et al., 2017).

2.4. Flow cytometry

Immune cells from the injured spinal cord were analyzed by flow cytometry. Spinal cord from mice treated with RvD1 or vehicle were harvested at day 1 ($n = 9$ per group), 3 (n = 5 per group) and 7 (n = 5 per group) after injury. Briefly, spinal cords were cut in little pieces and passed through a cell strainer of 70 μm (BD falcon) and the cell suspension was centrifuged twice at 300 *g* for 10 min at 4 °C. After cell counts, samples were divided, and cells alone and isotype-matched control samples were generated to control for nonspecific binding of antibodies and for auto-fluorescence. The following antibodies from eBioscience were used at 1:250 concentrations: CD45-PerCP, CD11b-PE-Cy7, Gr1-PE, Ly6C-FIC or APC, F4/80-APC Cy7 or PE, CD3-FITC, CD4-APC, CD8-PE and CD19-Pacific Blue. After 30 min of incubation with combinations of antibodies at 4 °C, the samples were washed and fixed in 1 % paraformaldehyde. For intracellular staining, cells were permeabilized with Permeabilization Wash Buffer (Biolegend) followed by staining unconjugated rabbit antibodies against iNOS (1:200 Abcam) and goat antibodies against Arg1 (1:200 Santa Cruz). After 30 min of incubation with combinations of antibodies at 4 °C, cells were washed and stained with Alexa488 or Alexa647 conjugated donkey secondary antibodies against rabbit or goat (1:750 Molecular Probes) for 30 min. Finally, the samples were washed and fixed in 1 % paraformaldehyde.

To perform the analysis, we first did singlet gating (doublet exclusion) for CD45 to ensure that only infiltrating leukocytes and resident microglia are selected, and then, the following combination of markers were used to identify CD4 T-Cells ($CD45^+$, $CD11b^-$, $CD3^+$, $CD4^+$), CD8 T Cells ($CD45^+$, CD11b, $CD3^+$, $CD8^+$), B cells ($CD45^+$, $CD11b^-$, $CD3^-$, $CD19^+$), microglial cells ($CD45^{low/med}$, $CD11b^+$, $F4/80^+$), monocytes/macrophages ($CD45^{high}$, $CD11b^+$, $F4/80^+$), and neutrophils ($CD45^{high}$, $CD11b^+$, $F4/80^-$, $Gr1^+$). Kinetic analysis of these immune cell types were calculated as described previously (Francos-Quijorna et al., 2017; Prüss et al., 2011). To study the phenotype of monocyte/macrophages, these cells were further differentiated based on Ly6C, CD16/32, iNOS, CD206 and Arg1 expression. Cells were analyzed using FlowJo® software on a FACSCanto flow cytometer (BD Biosciences).

2.5. Functional assessment

Locomotor recovery was evaluated at 1, 3, 5, 7, 10, 14, 21 and 28 days post-injury (dpo) in an open-field test using the nine-point Basso Mouse Scale (BMS), which was specifically developed for locomotor testing after contusion injuries in mice (Basso et al., 2006). The BMS analysis of hindlimb movements and coordination was performed by two independent assessors and the consensus score taken. The final score is presented as mean ± SEM.

At the end of the follow up period (day 28 post-injury), a

computerized assessment of locomotion was also performed using the DigiGait™ Imaging System (Mouse Specifics Inc., Boston, MA). This system is constituted of a motorized transparent treadmill belt and a high-speed digital video camera that captures images of the underside of the feet in walking animals. DigiGait™ software generates "digital pawprints" and dynamic gait signals, representing the temporal record of paw placement relative to the treadmill belt. This locomotor test allows for an easy and objective analysis of both static and dynamic locomotor parameters. Finally, the highest speed at which each mouse was able to walk was also recorded on the DigiGait treadmill belt. Briefly, each mouse was allowed to explore the treadmill compartment, with the motor speed set to zero, for 5 min. Then speed was gradually increased from 0 up to 35 cm/s and the maximum speed at which each mouse performed for at least 5 s was recorded (Francos-Quijorna et al., 2017; Santos-Nogueira et al., 2015).

2.6. Electrophysiological analysis

At day 28, electrophysiological tests were performed to evaluate spared central motor pathways after SCI. Motor evoked potentials (MEPs) were recorded from the *tibialis anterior* (TA) and *gastrocnemius* (GC) muscles with microneedle electrodes, in response to transcranial electrical stimulation of the motor cortex by single rectangular pulses of 0.1 ms duration. Pulses were delivered through needle electrodes inserted subcutaneously, the cathode over the skull, overlying the sensorimotor cortex, and the anode at the nose (Santos-Nogueira et al., 2015). Compound Muscle Action Potential (CMAP) M waves from tibialis anterior and gastrocnemius muscles were recorded for internal control of peripheral normal conduction. In this case the sciatic nerve was stimulated percutaneously by means of single pulses of 0.02 ms duration (Grass S88), delivered through a pair of needle electrodes placed at the sciatic notch (Francos-Quijorna et al., 2017). All potentials were amplified and displayed on a digital oscilloscope Tektronix 450S (Tektronix, OR) at settings appropriate to measure the amplitude from baseline to the maximal negative peak. To ensure reproducibility, the recording needles were placed under microscope to secure the same placement on all animals guided by anatomical landmarks. During the tests, the body temperature was kept constant by means of a thermostated heating pad.

2.7. Histological analysis

At 28 dpo, mice were deeply anesthetized using Dolethal (pentobarbital sodium; Vétoquinol E. V. S. A.) and perfused with 4 % paraformaldehyde in 0.1 M phosphate buffer. A 10 mm length of spinal cord c centered on the lesion site was harvested, post-fixed for 1 h in 4 % paraformaldehyde in 0.1 M PB and cryoprotected with 30 % sucrose in 0.1 M PB at 4 °C, for a minimum of 48 h. Spinal cords were fast-frozen at −60 °C in cryoembedding compound (Tissue-Tek® OCT, Sakura) and cut on a cryostat (Leica). Ten series of 10 μm thick sections were picked up on glass slides. Adjacent sections on the same slide were therefore 100 μm apart.

For demyelination analyses, sections were stained with Luxol Fast Blue (Sigma). For neuronal and axonal assessment, sections were incubated overnight at 4 °C with biotinylated antibodies against NeuN (1:200, Millipore) and NF (1:1000, Millipore), respectively. Moreover, double immunostaining for NF and MBP (1:100; Abcam) was done to assess the sparing of myelinated axons. Sections were incubated for 1 h at room temperature with the streptavidin-Alexa 594 conjugated or donkey anti-rabbit Alexa 594-conjugated antibodies (Molecular Probes, 1:500), and then coverslipped in Mowiol containing DAPI to label nuclei.

Tissue sections were viewed with Olympus BX51 microscope and images were captured using an Olympus DP50 digital camera, and using the CellˆA Image acquisition software. The epicenter of the injection or contusion injury impact was determined for each mouse spinal cord by localizing the tissue section with the greatest damage using LFB-stained section. Myelin sparing after SCI was calculated by delineating the spared LFB-stained tissue. Neuronal survival was assessed by counting the number of $NeuN^+$ cells in the ventral horns at the injury epicenter and at rostral and caudal areas. Axonal sparing was calculated by counting the number of axons in the dorsal column at the injury epicenter, the most damaged area of the spinal cord. The same sections were used to examine axonal demyelination in the dorsal column by counting the fibers double stained for NF and MBP at the lesion epicenter. The NIH ImageJ software was used to quantify all the histological parameters.

2.8. RNA isolation, reverse transcription, and real-time PCR

Uninjured control mice, and injured animals treated with vehicle or RvD1 ($n = 5$ per group) were euthanized with Dolethal (pentobarbital sodium, Vetoquinol; 0.01 ml/10 g, intraperitoneal) at 7 dpo, and perfused with vehicle buffer. A 5 mm segment of spinal cord centered on the lesion epicenter was harvested and rapidly frozen, and storage at −80 °C until mRNA extraction. For mRNA extraction, tissue was homogenized with Quiazol lysis reagent (Qiagen) and mRNA extracted using RNeasy Lipid Tissue kit (Qiagen), according to the user's guide protocol. An additional step with DNase I digestion (Qiagen) was included to avoid genomic DNA contamination.

1 μg mRNA of each sample was primed with Random Hexamers (Promega) and reverse transcribed using Omniscript RT kit (Qiagen). RNase inhibitor (Roche) was added (1 U/ μl final concentration) to avoid RNA degradation. RT-PCR reactions were performed using Brilliant III Ultra-Fast SYBR Green QPCR Master Mix (Agilent Technologies) according to the manufacturer's instructions. Data analysis was performed using the MyiQ Single-Colour Real-Time PCR Detection System (Bio-Rad laboratories). Primer sequences included the following: iNOS forward 5′-GGCCAGCCTGTGAGACCTTT-3′, iNOS reverse 5'-TTGGAAGTGAAGCGTTTCG-3′. Glyceraldehyde 3-phosphate dehydrogenase (GAPDH) was used as a housekeeping gene: GAPDH forward 5'-TCAACAGCAACTCCCACTCTTCCA-3′, GAPDH reverse 5'-ACCCTGTTGCTGTAGCCGTATTCA-3′. The amount of cDNA was calculated based on the threshold cycle (CT) value and was standardized by the amount of housekeeping gene using the 2-ΔΔC method (Livak and Schmittgen, 2001).

2.9. Microarray

Microarray hybridization was performed by the Scientific and Technical Support Unit and the Statistics and Bioinformatics Unit at the Vall D'Hebron Research Institut (Hospital de la Vall d'Hebron, Barcelona). mRNA samples of spinal cords harvested from uninjured mice ($n = 4$), as well as from 1 (vehicle n = 4; RvD1 $n = 5$) and 7 1 (vehicle n = 4; RvD1 n = 5) days post-injured animal treated with vehicle and RvD1 were processed for Affimetrix MOUSE Exon/Gene 2.1 ST chip array according to the manufacturer protocol. The optical images of the hybridized chip were processed with the Expression Console software (Affimetrix). CEL files containing the intensity values associated to probes and grouped into probe sets were obtained. Then, RMA method (Irizarry et al., 2003) was used to transform intensity values to expression values. RMA is a three step-method that integrates background adjustment, scaling and aggregation of the probe sets to remove non-biological elements of the signal and genes with low signal (those genes whose mean signal in each group did not exceed a minimum threshold) and low variability (genes whose standard deviation between all samples did not exceed a minimum threshold). The selection of differentially expressed genes between conditions was based on a linear model analysis with empirical Bayes moderation of the variance by Smyth (Smyth Gordon, 2004) and implemented in the limma Bioconductor package. In order to minimize type I errors (incorrectly rejected null hypotheses), all statistical tests were adjusted for multiple

comparisons using the Benjamini-Hochberg (Benjamini and Hochberg, 1995) Procedure, unless otherwise specified. To assess statistical significance in changes in gene expression a cut-off p-value <0.05 was used. All the statistical analysis were done using the free statistical language R and the libraries developed for microarray data analysis by the Bioconductor Project (www.bioconductor.org)

To investigate the biological meaning, term enrichment (over-representation) analysis (ORA) was performed against different pathway libraries. Terms were classified by functional annotation clustering analysis, where the list of selected genes (differentially expressed genes - DEGs) was compared to a reference set (universe - Affimetrix chip probes after filtering and mapping). The functional annotation cluster was ranked from largest to smallest enrichment score (ES), based on hypergeometric test and pathways sorted by statistical significance (typically, adjusted p-value). All plots were produced using different variations of the ggplot2 package (Wickham, 2016) and ORA pathway analyses were contrasted against KEGG (Kanehisa, 1997) Reactome (Gillespie et al., 2022), wikiPathways (Martens et al., 2020) and Gene Ontology (Mi et al., 2019) gene libraries, using DOSE (Yu et al., 2015) and ClusterProfiler (Wu et al., 2021) libraries. The microarray dataset is available under accession number GSE284533 in the Gene Expression Omnibus (GEO) database.

2.10. Experimental autoimmune encephalomyelitis

Adult female C57BL/6 mice (8–10 weeks old, Charles River Laboratories) were sedated with an intramuscular injection of ketamine (22 mg/kg, Imalgen 1000, Merial) and xylazine (2.5 mg/kg, Rompun, Bayer). EAE was induced via subcutaneous immunization with 300 μg of myelin oligodendrocyte glycoprotein peptide 35–55 (MOG35–55, MEVGWYRSPFSRVVHLYRNGK, Thermo Fisher Scientific, MA, USA) in 200 μl Complete Freund's Adjuvant (CFA, Difco, MI, USA), supplemented with 4 mg/ml heat-inactivated *Mycobacterium tuberculosis* (Difco, MI, USA). Additionally, mice received intraperitoneal injections of 400 ng of pertussis toxin (Sigma-Aldrich, ON, USA) in 100 μl sterile saline at the time of induction and again 48 h later (Sanchez-Fernandez et al., 2019).

Mice were scored daily from day 0 to day 21 post-EAE induction, with the researcher blinded to experimental groups during functional assessments. EAE clinical signs were evaluated using a 6-point scale: 0 = normal walking, 0.5 = partially paralyzed tail, 1 = fully paralyzed tail, 2 = mild hind limb weakness with quick righting reflex, 3 = severe hind limb weakness with slow righting reflex, unable to bear weight, 3.5 = severe hind limb weakness with partial hind limb paralysis, 4 = complete paralysis of at least one hind limb, 4.5 = complete paralysis of one or both hind limbs with trunk weakness, 5 = complete hind limb paralysis with forelimb weakness or paralysis, and 6 = moribund.

Following EAE induction, mice were randomly assigned to treatment and control groups. Starting from the first day of clinical symptom onset, daily intraperitoneal injections of 1 μg RvD1 ($n = 10$) or vehicle ($n = 11$) were administered until the study concluded 21 days post-induction.

2.11. Statistical analysis

All analyses were conducted through GraphPad Prism 9.0. Data are shown as mean ± standard error of the mean. Maximal speed on a treadmill was analyzed using the Mantel-Cox test. Functional follow-up for BMS score, EAE score, as well as histological analysis of myelin and neuronal sparing were analyzed using two-way repeated measure ANOVA with post-hoc Bonferroni's post-hoc test for multiple comparisons. Two-tailed Student's t-test was used for the single comparison between two groups. Differences were considered significant at $p < 0.05$. Microarray gene differential expression analysis and term over-representation analyses were performed as described above.

3. Results

3.1. RvD1 accelerates neutrophil clearance but fails to enhance inflammatory resolution program after traumatic spinal cord injury

Based on previous findings from our laboratory suggesting that the deficit in the resolution of inflammation following SCI may be linked to impaired synthesis of SPMs (Francos-Quijorna et al., 2017), we investigated the impact of systemic administration of RvD1 on immune cell clearance from the contused spinal cord. For this purpose, we first determined the effects of different doses of RvD1 on functional recovery after SCI to choose the optimal dose of RvD1 to conduct our experiments (Supplementary Fig. 1a-d). Since the three doses led to similar effects on locomotor recovery, we selected the dose of 1 μg per mouse and day, aligning with our previous work on MaR1 in SCI (Francos-Quijorna et al., 2017).

Flow cytometry analysis (Supplementary Fig. 2a) was used to compare the accumulation of immune cells in vehicle and RvD1-treated animals following SCI. We found that RvD1 treatment slightly reduced, although not to the significant level, the infiltration of neutrophils in the spinal cord at 1 dpo (Fig. 1a). However, after analyzing several resolution parameters (Fig. 1a), we found that RvD1 accelerated the clearance of these cells from the contused spinal cord. In particular, the resolution index (Ri) for neutrophils, which reflects the time required for the count of this leukocyte subset to decrease to 50 % from the peak of maximum accumulation, was reduced by 48 % following RvD1 treatment. Contrary to our expectations, by day 7, when neutrophil counts typically reach a resolution plateau in SCI, the number of neutrophils remaining in the lesioned spinal cord was similar between RvD1-treated and vehicle-treated mice (Fig. 1a). This suggests that, while RvD1 accelerated neutrophil clearance initially, it did not enhance the overall reduction of this immune cell population in the injured spinal cord.

We then sought to examine the effect of RvD1 on microglia and various leukocyte subset counts after SCI (Fig. 1b, c and Supplementary Fig. 2b-d). Our results showed that RvD1 did not mitigate the accumulation of microglia or macrophage in the lesioned spinal cord (Fig. 1b, c), although it tended to reduce their counts. Similarly, RvD1 did not reduce the recruitment of different lymphocyte subsets into the spinal cord for the first 7 dpo (Supplementary Fig. 2b-d).

3.2. RvD1 treatment does not modulate macrophage polarization after SCI

Macrophages represent a heterogeneous population of cells with varying effects on damaged tissue based on their phenotype. Ly6C^{high} macrophages possess phagocytic and inflammatory properties, while Ly6C^{low} macrophages promote wound healing and repair(Arnold et al., 2007; Nahrendorf et al., 2007). Thus, in this study, we aimed to investigate the effect of RvD1 on Ly6C expression in macrophages after SCI. Our results showed that RvD1 did not alter the proportion of Ly6C^{low} and Ly6C^{high} macrophages after SCI (Fig. 2a-c).

We then assessed whether RvD1 modulated the expression of M1/M2-like markers in macrophages after SCI. Our data revealed that the M2-like marker, Arg1, was barely detectable in macrophages after 7 days post-lesion (<3 %) and that RvD1 treatment failed to enhance its levels (Fig. 2d, e). Similarly, the levels of another M2-like marker, CD206, was not modulated by RvD1 (Supplementary Fig. 3b). On the other hand, the expression of the M1-like marker, iNOS, was slightly reduced in RvD1-treated mice, either by assessing the percentage of iNOS+ macrophages (61 ± 1 vs 53 ± 4 % in vehicle- and RvD1-treated mice, respectively) and the median fluorescence intensity (MFI; 648 ± 120 vs 470 ± 141 in vehicle- and RvD1-treated mice, respectively). However, this reduction did not reach statistical significance (Fig. 2d, e). Lack of iNOS reduction by RvD1 treatment was further confirmed by RT-qPCR analysis of iNOS transcript levels (Supplementary Fig. 3a). Moreover, flow cytometry analysis also showed that the expression of

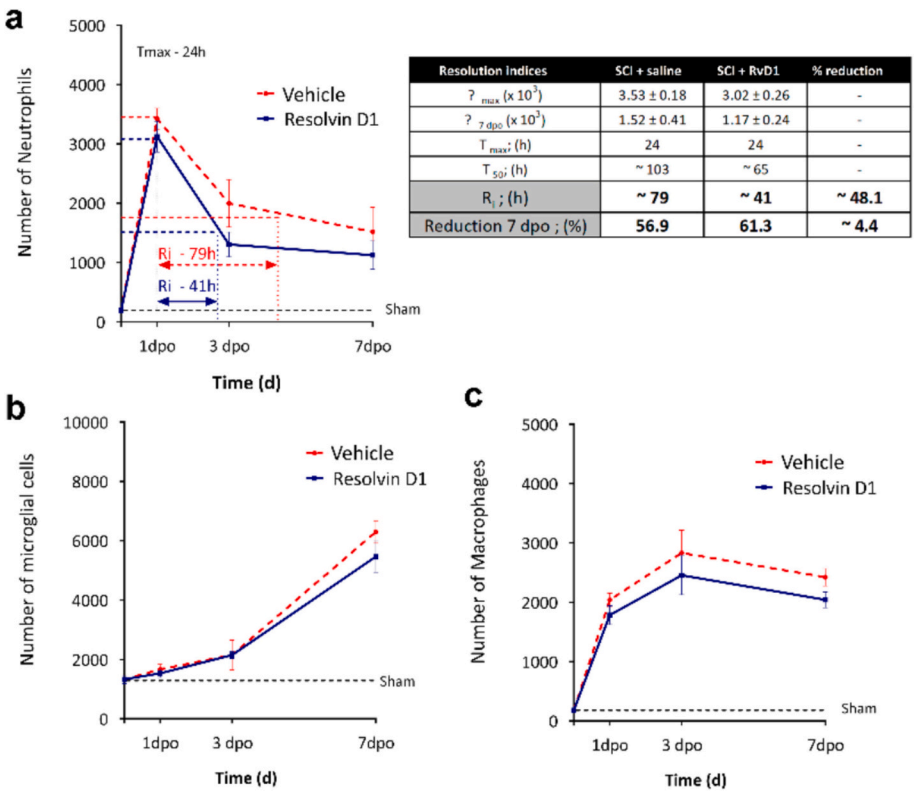

Resolution indices	SCI + saline	SCI + RvD1	% reduction
? max (x 10³)	3.53 ± 0.18	3.02 ± 0.26	-
? 7 dpo (x 10³)	1.52 ± 0.41	1.17 ± 0.24	-
T max; (h)	24	24	-
T 50; (h)	~ 103	~ 65	-
Ri ; (h)	~ 79	~ 41	~ 48.1
Reduction 7 dpo ; (%)	56.9	61.3	~ 4.4

Fig. 1. Effects of RvD1 in the infiltration of immune cells after SCI. (A) Graph showing neutrophil recruitment and resolution indices. Inset shows some inflammatory kinetics measurement, which include: ψmax = maximal cell counts; ψ7 = cell counts at 7 dpo; Tmax, time after SCI until reaching max cell numbers, T50, time after SCI until reduction of cell numbers by 50 %; and Ri. (B—C) Graphs showing quantification of (B) microglial cells and (C) macrophages, following SCI at 1, 3 and 7 dpo with or without RvD1 treatment. Results were assessed for normality using the Shapiro–Wilk test and two-way ANOVA with Bonferroni's post hoc test was used to analyze significant differences in the dynamics of neutrophil, microglial cells and macrophages counts after SCI; *t*-test was used to assess the different inflammatory kinetic indices ($n = 9$ at 1 dpo, $n = 5$ at 3dpo and n = 5 at 7 dpo per group). Error bars indicate SEM.

another M1-like marker, CD16/32, remained unaltered after RvD1 treatment (Supplementary Fig. 3b). Therefore, our results suggest that RvD1 fails to shift macrophages from a pro-inflammatory to an anti-inflammatory/pro-repair state after SCI.

3.3. RvD1 does not attenuate the expression of pro-inflammatory cytokines in SCI

After investigating the impact of RvD1 on the recruitment and phenotype of immune cells after SCI, we proceeded to examine the effect of RvD1 on the protein levels of various cytokines in the spinal cord at 24 h post-lesion. Luminex assay revealed that the expression of most cytokines was unaltered in the injured spinal cords harvested from mice treated with RvD1 (Fig. 3). However, the expression of two chemokines that are critical for recruiting immune cells into challenged tissues, CCL11 and CXCL10, was significantly increased by RvD1 treatment (27.3 ± 4.5 and 38 ± 2 pg/mg protein for CCL11; and 1517.7 ± 236.4 and 2302.1 ± 136.6 pg/mg protein for CXCL10 in vehicle and RvD1 treated mice, respectively). Conversely, the anti-inflammatory cytokine IL-13 was significantly reduced in animals receiving RvD1 (4.6 ± 0.8 and 2.9 ± 0.2 pg/mg protein in vehicle vs RvD1).

3.4. Administration of RvD1 does not improve functional outcomes after SCI

We then investigated the efficacy of RvD1 as a therapeutic option in SCI by assessing its impact on functional recovery. BMS analysis revealed that RvD1 treatment failed to improve locomotor function of the animals (score 3.8 ± 0.19 vs 3.55 ± 0.26 in vehicle and RvD1 groups, respectively) (Fig. 4a). Indeed, the proportion of animals that exhibited plantar placement with occasional stepping was reduced in the RvD1-treated group (BMS ≥4; 40 % RvD1 vs. 70 % vehicle animals) (Fig. 4b).

At the end of the follow up period (day 28 post-injury), we further assessed locomotor function by doing DigiGait analysis. These experiments showed that RvD1-treated mice tended to display slower locomotion on a treadmill (Fig. 4c, d). In addition, those animals that were able to locomote at speed of 14 m/s on a treadmill (Fig. 4e, f) showed some alterations in various locomotor parameters such as stride length variability, paw area at peak stance, and stride frequency of Max dA/dT after RvD1 treatment (Fig. 4g-j).

We also assessed, by electrophysiological methods, the preservation of the spinal cord descending pathways at day 28 post-injury. Motor evoked potentials (MEPs) demonstrated no notable differences in MEP latency or amplitude between the RvD1-treated and control groups (Fig. 5a, c, and 5b, d), indicating that RvD1 administration does not improve the preservation of descending spinal motor pathways.

In summary, these results clearly indicate that the administration of RvD1 does not improve functional outcomes after SCI.

3.5. Treatment with RvD1 does not reduce secondary tissue damage after SCI

We then evaluated the efficacy of RvD1 in mitigating tissue damage after SCI. For this purpose, histological tissue sections of the injured spinal cord were processed to evaluate different histopathological parameters. Luxol Fast Blue (LFB) stained sections revealed that RvD1 treatment did not reduce myelin loss ($p > 0.05$, RM two-way ANOVA) (Fig. 6a, b). Additionally, quantification of NeuN+ cells in the ventral horns of the spinal cord showed no significant increase in neuronal

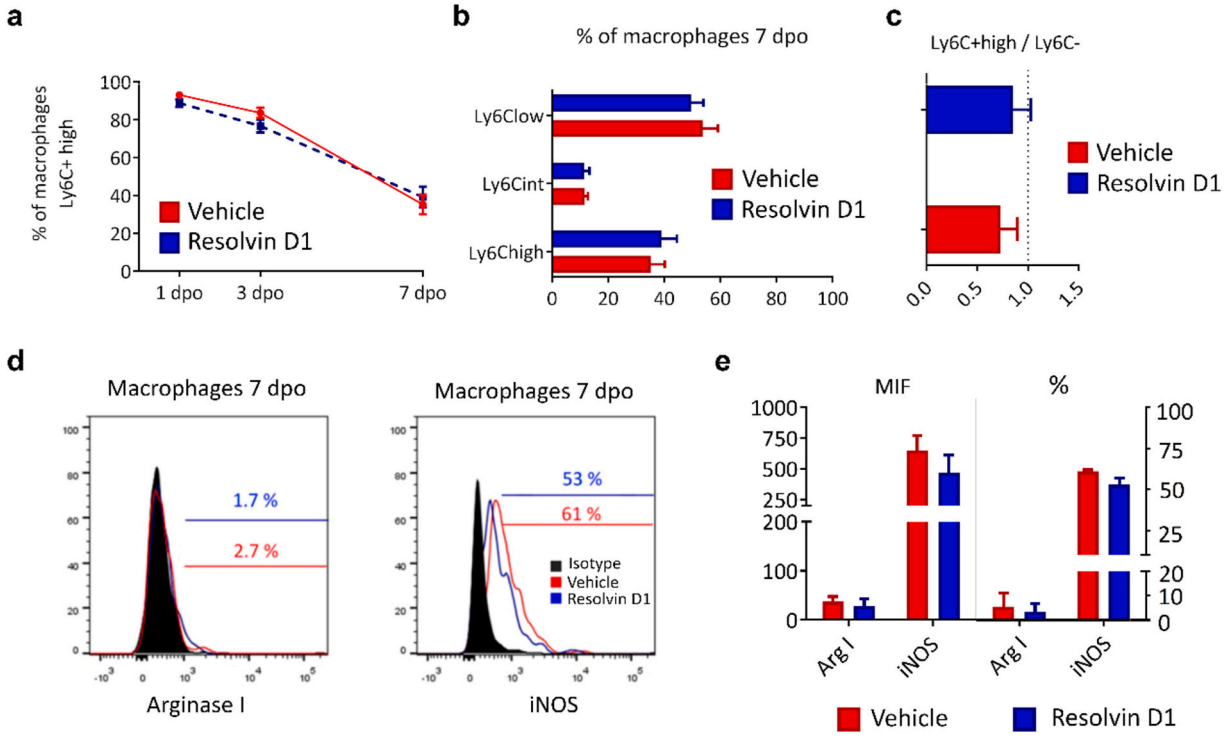

Fig. 2. Impact of RvD1 treatment on macrophage phenotypic modulation after SCI. (A) Graph showing the evolution of LyC6^{high} macrophages in the injured spinal cord after RvD1 treatment. (B) Graph showing proportion of different macrophage subsets in the injured spinal cord at 7 dpo. (C) Graph showing the effects of RvD1 in the ratio of LyC6^{high}/LyC6^{low} macrophages in the injured spinal cord at 7 dpo. (D-E) Representative FACS histograms plots of (D) Arg I and (E) iNOS expression in macrophages at 7 dpo. (F) Graph showing the expression of Arg1 and iNOS assessed by mean fluorescence intensity (MFI) and percentage in macrophages after SCI. Mean ± SEM. (n = 5 per group). Student t-test was used to analyze significant differences between RvD1 and control mice.

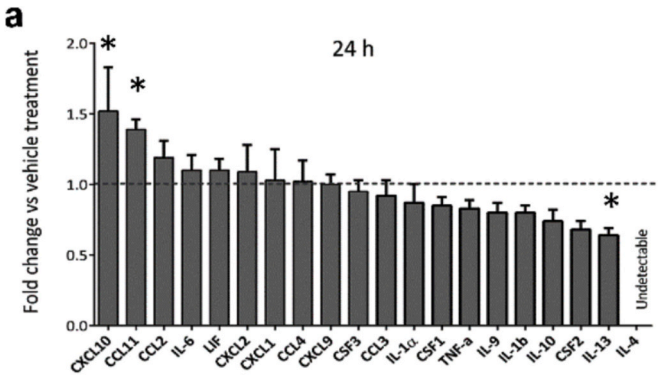

Fig. 3. Pro-inflammatory cytokine expression levels after SCI in RvD1 treated animals compared with the control group. (A) Multiplex analysis of cytokine protein levels from spinal cord of RvD1-treated and vehicle-treated mice at 24 h post-injury. Mean ± SEM. (n = 5 per group) *p < 0.05 vs vehicle. Student t-test was used to analyze significant differences between RvD1 and control mice.

preservation after RvD1 treatment (Fig. 6c, d). Furthermore, to determine the impact of RvD1 treatment on axonal and myelin preservation, we quantified the number of axons (NF+) and those with preserved myelin sheath (NF/MBP+) in the dorsal columns at the injury epicenter, the most damaged area of the spinal cord. This analysis revealed that RvD1 treatment did not result in a significant preservation of axons or myelin after SCI (Fig. 6e, f).

Overall, these findings provide clear evidence that the administration of RvD1 does not result in improved histological outcomes after SCI.

3.6. RvD1 treatment does not modify the expression of genes related to inflammatory pathways

To comprehensively assess the molecular impacts of RvD1 treatment on mice following SCI, we conducted microarray-based expression profiling experiments on the injured spinal cord tissue at both day 1 and 7 post-injury (Fig. 7a).

Preliminary validation of the data suggested that, transcriptionally, RvD1-treated and untreated animals are similar after SCI, as evidenced by Principal Component Analysis (Fig. 7b) and sample similarity studies (Supplementary Fig. 4a). Nevertheless, we further explored the effects of RvD1 treatment at a more refined level to gain a deeper understanding of its impact following SCI.

We initially examined the impact of the injury itself in the first week following SCI in mice and determined whether the resulting responses were time-specific or consistently altered during the acute (1 day) and sub-acute (7 day) phases (Supplementary Fig. 4). We observed distinct transcriptional changes in the spinal cords of injured versus non-injured animals, with samples segregating into two distinct groups at both 1 and 7 days after injury (Supplementary Fig. 4a). Due to the massive differences between pre- and post-SCI conditions, a more stringent differential expression analysis was performed using *Benjamini*-Hochberg correction for multiple comparisons (adjusted p-value/FDR < 0.01) and an abs (log2)FC > 1 to select greater biological changes. This analysis revealed 647 and 1210 differentially-expressed genes at 1- and 7 dpo, respectively, with 271 genes being commonly differentially expressed at both time points (Supplementary Fig. 4 b and c).

Further pathway analysis demonstrated that pathways related to extracellular matrix alteration and cell migration were primarily modulated at 1 day after SCI (Supplementary Fig. 4 d-f), whereas changes in immune responses were more prevalent at 1 week after SCI (Supplementary Fig. 4 g-i). Additionally, cell proliferation pathways were found to be altered at both time points, suggesting sustained

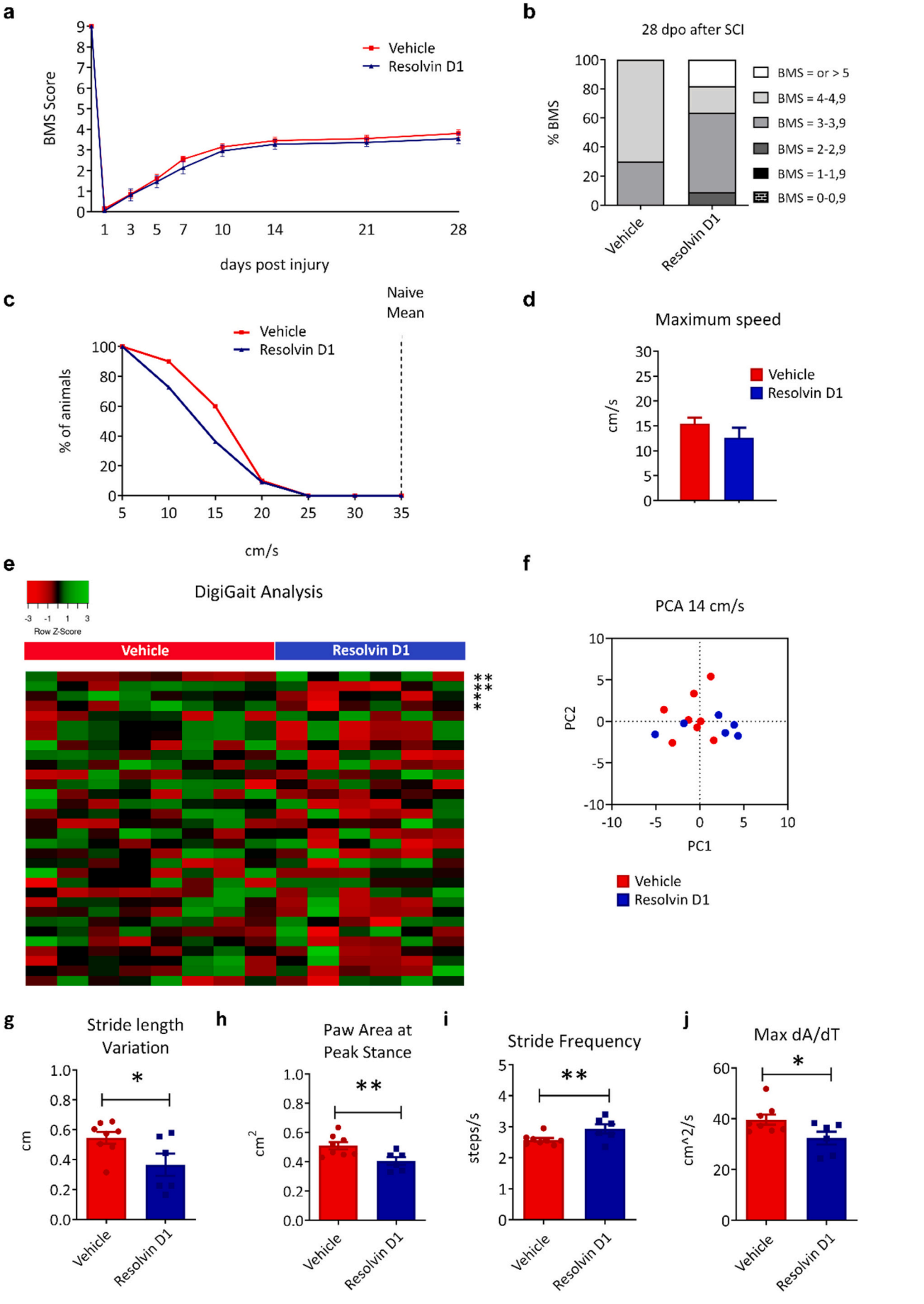

(caption on next page)

Fig. 4. Functional recovery analysis after RvD1 treatment after SCI. Animals treated with RvD1 did not show significant improvement in locomotor skills after SCI, assessed by (A-B) the 9-point Basso Mouse Scale (BMS) or (C-J) DigiGait™ Imaging System. (A) Graph showing the BMS score of RvD1 and vehicle treated mice after SCI. (B) Bar graph showing the percentage of mice in each stage of BMS scale. (C) Graph and (D) bar graph showing maximum locomotion speed differences between groups after SCI. (E) heatmap showing the effect of RvD1 treatment 28 days after SCI assessed by DigiGait™ Imaging System. (F) PCA of animal posture, balance and coordination parameters in mice treated with or without RvD1. (G-J) Bar graph showing the only 4 gait parameters with significant differences between groups. Data are expressed as mean ± SEM. *$p < 0.05$ Results were assessed for normality using the Shapiro–Wilk test and analyzed using two-ways RM-ANOVA with Bonferroni's post hoc test in (A), Mantel-Cox test in C and *t*-test in E, G-J (A-D $n = 8$ in vehicle group, $n = 10$ in RvD1 group; *E*-J n = 8 in vehicle group, $n = 6$ in RvD1 group).

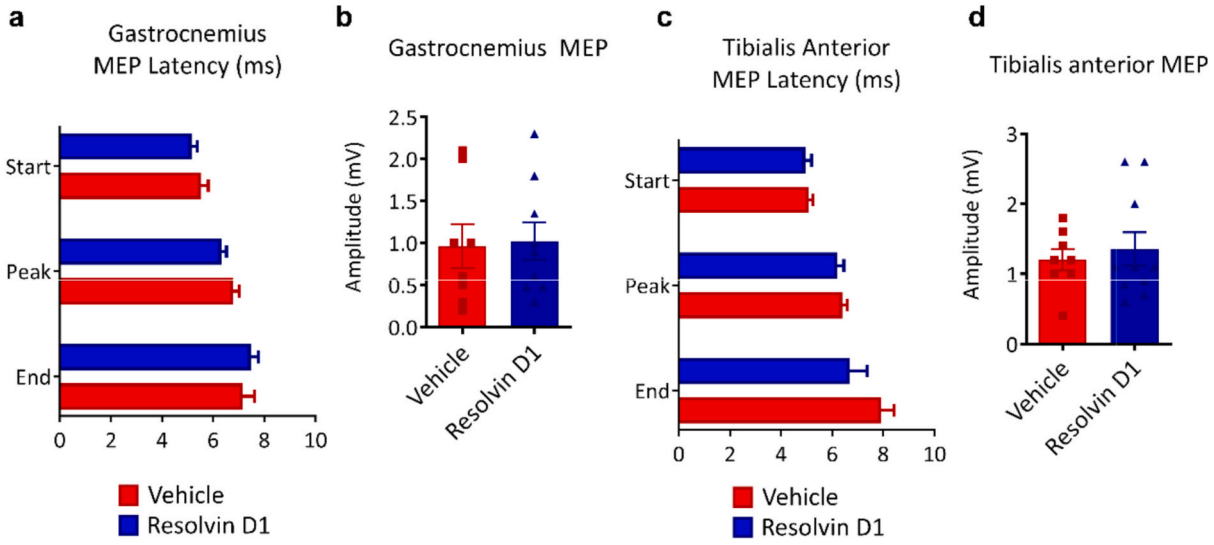

Fig. 5. Electrophysiology analysis after SCI. RvD1 treatment does not improve MEPs after SCI. (A-D) Quantification of MEPs latency and amplitude recorded from the gastrocnemius (A-B) and tibialis anterior muscles (C—D) after SCI. Data are shown as mean ± SEM. (*$p < 0.05$; *t*-test; n = 8 in vehicle- and n = 10 in RvD1-treated mice).

alteration of these pathways during the first week after SCI (data non shown).

We then further characterized the impact of RvD1 treatment on the differential expression of genes at day 1 and day 7 following SCI. Differential expression analysis revealed there were no differences between RvD1-treated and control mice at both 1- and 7-days-post-SCI when results were adjusted for multiple comparisons (Benjamini-Hochberg Procedure). The RvD1 responses at day 1 post-injury were almost indistinguishable from those observed in vehicle injured animals (Supplementary Fig. 5 a-c). Nevertheless, in an attempt to elucidate possible underlying differences occurring between treatments we performed differential expression analysis and fixed statistical significance at (unadjusted for multiple comparisons) *p*-value <0.01 or < 0.05. Using these parameters, we observed that only 50 and 300 genes were differentially expressed, respectively, in RvD1- versus vehicle-treated mice (Extended data - Table 1). Notably, most of these genes correspond to annotated sequences with not known function (Riken, ORFs), pseudogenes (Gms) or microRNAs (Supplementary Fig. 5 b, d and e). Pathway analysis (unadjusted p-value <0.05) revealed minimal differences at immune signaling events (Supplementary Fig. 5f).

Finally, we assessed the differential gene expression between RvD1 and vehicle-treated mice at 1-week post-SCI, time-point when inflammatory resolution is needed to avoid tissue damage. At this stage, the differences between the two groups were slightly more pronounced than those observed at day 1, with the samples being segregated into two distinct groups based on treatment (Fig. 7c, d). RvD1 treatment resulted in the differential expression of approximately 450 and 1500 genes with an unadjusted p-value of <0.01 or < 0.05, respectively, with a nearly balanced distribution of up- and down-regulated genes (Extended data - Table 2). Interestingly, none of the top 10 up- or down-regulated genes in RvD1-treated mice compared to the control group (by p-value) were associated with the inflammatory response at 7 days post-SCI (Fig. 7 e-g). In-depth pathway analysis of all statistically significant differentially expressed genes (RvD1 vs. vehicle) at 1-week post-SCI revealed downstream metabolic effects (ribosomal functions) and differences in extracellular matrix pathways (Fig. 7h).

In conclusion, our new findings in line with our previous results, support the notion that the administration of exogenous RvD1 after SCI in mice fails to resolve inflammation.

3.7. Lack of RvD1 receptor overexpression in sub-acute stage of inflammatory response after SCI

To shed light on the lack of efficacy of RvD1 treatment in resolving the inflammatory response following SCI, we conducted an analysis of the expression of its receptors at various time points post- injury. Specifically, we focused on the Formyl peptide receptor 2 (ALX/FPR2), the only known RvD1 receptor in mice, as no murine homologs of the human GPR32 receptor has been described(Bäck et al., 2014). Our findings indicate that the expression of FPR2 is significantly increased in the injured spinal cord parenchyma at day 1 post-injury and tends to normalize its levels by day 7 (Fig. 8a). However, RvD1 treatment prevented the induction of FPR2 in the injured spinal cord (Fig. 8a).

This may indicate that the lack of efficacy of RvD1 treatment in resolving the inflammatory response after SCI may be, at least in part, by the effects of RvD1 on preventing the induction of ALX/FPR2 transcripts in the injured spinal.

We next assessed whether the prevention of ALX/FPR2 upregulation in the lesioned spinal cord observed by RvD1 treatment was responsible for the lack of therapeutic efficacy of this SPM in spinal cord contusion. For this purpose, we initiated RvD1 administration on day 1 post-injury, thereby avoiding the acute impact of RvD1 on ALX/FPR2 expression. This experiment revealed that, unlike treatment initiated at 1 h post-injury, animals receiving RvD1 treatment at 1 day following SCI resulted in a trend towards improved locomotor performance, although the effect did not reach statistical significance (Fig. 9a, b).

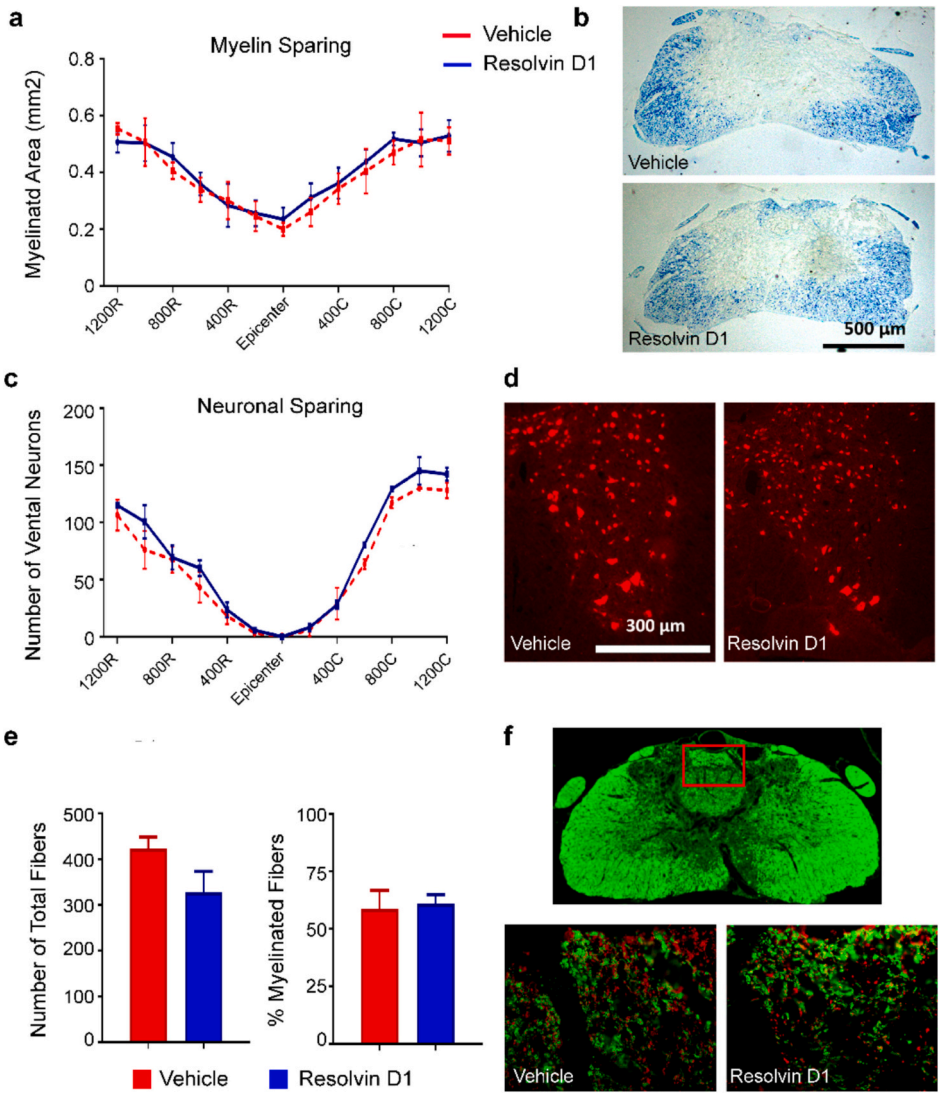

Fig. 6. Histological analysis of injured spinal cords after RvD1 treatment. (A) Quantification of myelin sparing at various distances rostral and caudal to the injury epicenter. (B) Representative micrographs showing myelin sparing at the injury epicenter in sections stained with LFB from saline- and RvD1-treated mice. (C) Quantification of ventral horn neuron survival at various distances rostral and caudal to the injury epicenter reveals the lack of effect of RvD1 in neuronal survival. (D) Representative micrographs showing sparing of ventral horn neurons in saline- and RvD1-treated mice tissue in sections stained against NeuN at 800 µm rostral to the injury epicenter. (E) Quantification of dorsal neurofilament and MBP immunoreactivity at the injury epicenter. (F) Representative micrographs showing dorsal neurofilament (red) and MBP staining at the injury epicenter from saline- and RvD1-treated mice. Data are expressed as mean ± SEM. (*$p < 0.05$; two-ways RM-ANOVA, Bonferroni's post hoc test in A, and D; t-test in F; $n = 5$). (For interpretation of the references to colour in this figure legend, the reader is referred to the web version of this article.)

Previous studies have demonstrated the therapeutic effects of RvD1 in various conditions, including EAE, a mouse model of multiple sclerosis (Poisson et al., 2015; Zhang et al., 2024). To determine whether the lack of beneficial actions of RvD1 was specific to SCI we investigated its actions in EAE. This experiment revealed that daily administration of RvD1 starting at the onset of the disease, ameliorated the neurological deficits of EAE mice (Fig. 9c). These findings suggest that the therapeutic potential of this pro-resolving agonist cannot be applicable across all the pathological conditions but may instead be effective in specific disorders.

4. Discussion

Timely resolution is the ideal outcome of acute inflammation, as it is required for ensuring return to tissue homeostasis and host health. It is now appreciated that resolution of inflammation is not a passive process as it was once thought. This is indeed controlled, in part, by the biosynthesis of SPMs derived from poly-unsaturated fatty acid (PUFA) (Serhan and Petasis, 2011). SPMs actively turn off the inflammatory response by acting via distinct G protein-coupled receptors expressed on immune cells that mediate dual anti-inflammatory and pro-resolution programs (Buckley et al., 2014; Serhan et al., 2015). Nevertheless, when the synthesis of SPMs is defective or delayed, inflammation may become chronic, cause bystander effects, and contribute to the pathogenesis of many highly burdening diseases. This is the case of SCI where, previous results from our laboratory (Francos-Quijorna et al., 2017) demonstrated that lesion milieu is characterized by impaired induction of SPMs, and administration of the DHA-derived SPM, MaR1, enhanced resolution of inflammation after SCI and improved functional and histopathological outcomes. Besides MaR1, there are other DHA-derived SPMs, which include the different members of the RvD series (RvD1-RvD6) and protectins (Bannenberg and Serhan, 2010; Serhan et al., 2008). Among them, RvD1 is the most studied member of this lipid family and has been shown to mediate potent effects in boosting the

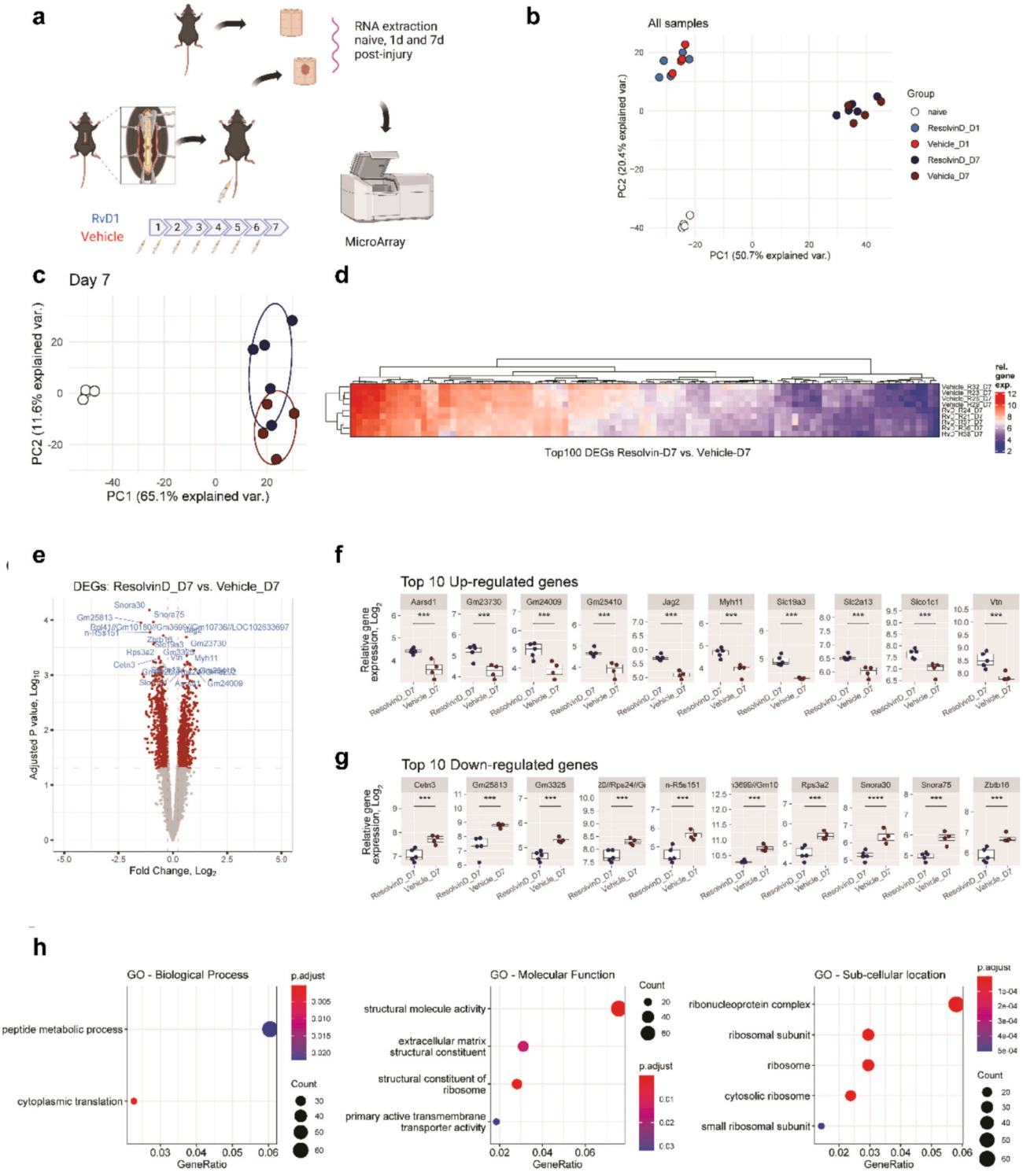

Fig. 7. Transcriptomic analysis of the injured spinal cord after RvD1 treatment. (A) Experimental design of transcriptomic analysis. (B) 2D Principal Component Analysis (PCA) of microarray data (filtered and normalized counts) comparing naive vs RvD and vehicle-treated animals at 1 and 7 days after SCI. PCA shows treatment separation between injured and uninjured samples and between 1 and 7 days after SCI but not between RvD1 and vehicle-treated animals. (C) 2D PCA comparing naive with control (vehicle) and RvD1-treated injured animals 1 week after SCI. Note that there are no significant differences between both treatments at this time-point. (D) Heatmap of top 100 differentially-expressed genes between RvD1-treated mice and vehicle-treated mice at 7 dpo. Minor but obvious changes can be observed between the two groups. In addition, Euclidean-distance analysis clusters samples by treatment group (y-axis dendrogram). (E) Volcano plot showing statistical significance and log2 fold-change (RvD1 vs vehicle) at 7dpo. A *p*-value threshold of 0.05 (dotted blue line) and an abs(log2FC) > 0.25 (dotted red line) were used to highlight the most relevant differentially expressed sequences. From this pool, shows the (F) Top 10 up-regulated (sorted by log2FC) and the (G) Top 10 down-regulated (sorted by statistical significance) sequences between RvD1 and vehicle-treated mice at 7 days post-SCI. (H) Over-representation pathway analysis (ORA) of differentially expressed unique genes (RvD1 vs control) matching Gene Ontology (Biological Process and Molecular Function) gene libraries. Significance scores are denoted as $^{**}p < 0.05$, $^{**}p < 0.01$, $^{***}p < 0.001$ and $^{****}p < 0.0001$. ($n = 4$ in naive and vehicle-treated groups and $n = 5$ in RvD1 groups). (For interpretation of the references to colour in this figure legend, the reader is referred to the web version of this article.)

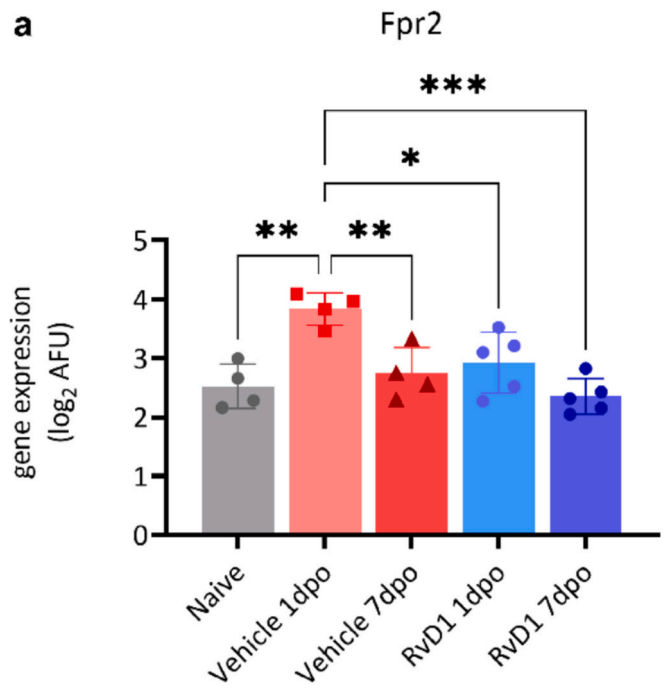

Fig. 8. Analysis of RvD1 receptor expression following SCI. (A) Bar-graph showing the expression of fpr2 gene within uninjured and injured spinal cord (1 and 7 dpo) in mice treated with vehicle and RvD1. Data are expressed as mean ± SEM. *$p < 0.05$; Results were analyzed using *t*-test ($n = 4$ in naive and vehicle-treated groups and $n = 5$ in RvD1 groups).

resolution of inflammatory in a wide spectrum of pathologies (Norling et al., 2012a; Norling et al., 2016), but not in neurotrauma yet. Therefore, in the present report, we wondered whether systemic RvD1 administration has similar therapeutic actions as MaR1 in acute SCI (Francos-Quijorna et al., 2017).

Unexpectedly, our study reveals that systemic administration of RvD1, at a dose of 1 μg/day for a week, does not lead to resolution of inflammation following SCI. A detailed flow cytometry analysis reveals that this SPM, consistent with previous studies, accelerates the clearance of neutrophils from the damaged spinal cord environment(Norling et al., 2012a). However, this effect is short-lived and only observed for the first 3 days after SCI but not thereafter. Furthermore, RvD1 fails to diminish the number of microglia and various leukocyte subsets after SCI and to redirect microglia and macrophages towards an anti-inflammatory phenotype. Instead, RvD1 increases the production of the pro-inflammatory cytokines CCL11 and CXCL10, while reducing the level of the anti-inflammatory cytokine IL-13. Notably, the absence of resolution of inflammation by RvD1 treatment after SCI is reflected in the lack of improvement in histological and functional outcomes.

To gain mechanistic insights into the poor resolution of inflammatory by RvD1 following SCI, we conducted microarray-based expression profiling. We used naïve instead of sham mice for the gene array analysis in SCI. While previous studies indicate that both laminectomy and impact trauma can induce gene expression changes, the alterations caused by laminectomy alone are relatively mild compared to those resulting from the impact trauma. However, we acknowledge that some of the transcriptomic changes observed in this study may be influenced by the absence of a sham-laminectomy control (De Biase et al., 2005).

Our findings showed that there were no significant differences in genes associated with the inflammatory response between injured spinal cords from mice treated with RvD1 and vehicle, and only differences in extracellular matrix and ribosomal function pathways were found at day 7 post-SCI. These results are consistent with our FACS analysis, which demonstrated that RvD1 did not lead to improved resolution of inflammation after SCI and did not confer protection against functional and tissue loss.

MaR1 and RvD1 are both derived from DHA, but while MaR1 treatment has been shown to promote beneficial inflammatory resolution (Francos-Quijorna et al., 2017), the mechanisms underlying RvD1's inability to do so after SCI remain unknown. Our current focus is on RvD1 receptor expression. It is well established that in human cells,

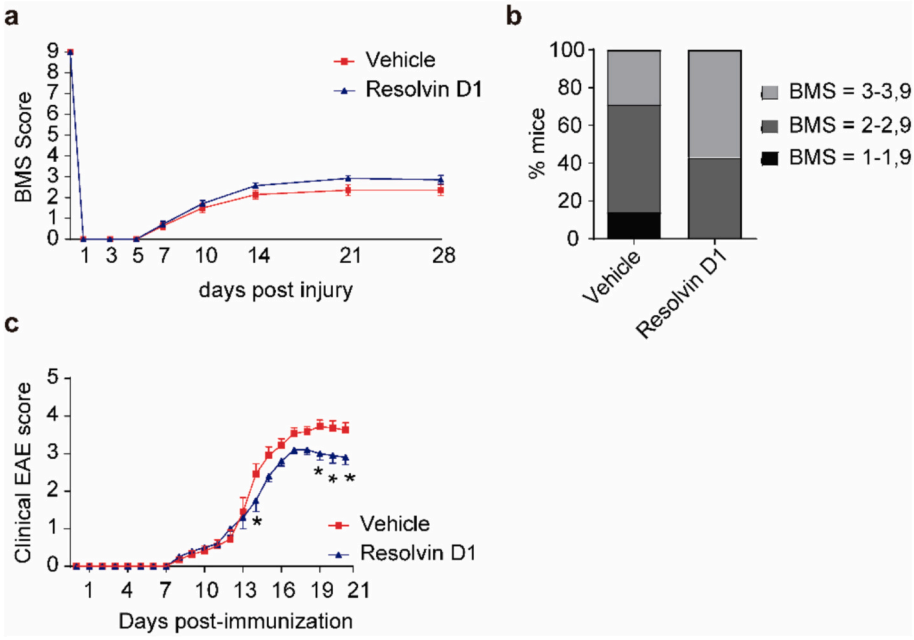

Fig. 9. Effects of delay treatment of RvD1 in SCI and EAE. (A) Graph illustrating the BMS scores of SCI mice treated with delayed RvD1 (1-day post-injury) compared to the vehicle-treated group. (B) A bar graph representing the percentage distribution of mice across different stages of the BMS scale. (C) A plot showing the neurological scores of EAE mice treated with RvD1, initiated at the onset of disease symptoms. Data are expressed as mean ± SEM. *p < 0.05 Results were assessed for normality using the Shapiro–Wilk test and analyzed using two-ways RM-ANOVA with Bonferroni's post hoc test in (A, C (A-B $n = 7$ in vehicle group, n = 7 in RvD1 group; C $n = 11$ in vehicle group, $n = 10$ in RvD1 group).

RvD1 acts through the Formyl peptide receptor 2 (ALX/FPR2) receptor and GPR32 receptor (Krishnamoorthy et al., 2010). However, since no murine homologs of the human GPR32 receptor exist, the effect of RvD1 in our SCI mouse model is limited to its effect through Fpr2, the murine homolog for ALX/FPR2.

The effect of RvD1 must be closely related to the specific time-expression of the receptor. Guo and collaborators showed that in a model of stroke, FPR2 expression increased after subarachnoid hemorrhage (SAH) and peaked at 24 h but reduced considerably later (Guo et al., 2016). In agreement with these findings, our microarray data shows that this receptor is induced in the injured spinal cord parenchyma at day 1 post-injury and tended to normalize its mRNA levels by day 7. However, RvD1 prevented the early induction of ALX/FPR2 in the injured spinal cord. In line with these results, the Godson group also showed that LXA4, another FPR2 ligand, induced a time-dependent internalization of the receptor from the plasma membrane to the intracellular space (Maderna et al., 2010). This could, at least in part, explain the lack of effectiveness of RvD1 when administered after SCI. This is indeed supported by a previous study revealing that RvD1 halted inflammation and exerted therapeutic actions after hemicerebellectomy in rats (Bisicchia et al., 2018) or in EAE in mice (Poisson et al., 2015; Zhang et al., 2024). In this line, we also show the beneficial effects of RvD1 in EAE suggesting that this SPM may be condition-specific, showing effectiveness in certain disorders rather than universally across all CNS pathological conditions.

In conclusion, we show for the first time that daily administration of RvD1 for 1 week after SCI fails to halt the inflammatory response, and does not induce improvements in functional and histopathological outcomes. This study therefore highlights that different SPMs may have divergent actions under different pathological conditions. Acquiring a better understanding of the different SPM will allow us to determine which of these might be suitable therapeutic targets for the treatment of SCI and other neurological conditions.

Ethical approval and consent to participate

All experimental procedures were approved by the Universitat Autònoma de Barcelona Animal Experimentation Ethical Committee (CEEAH 2878, 4057, 4751) and followed the European Communities Council Directive 2010/63/EU, and the methods were carried out in accordance with the approved guidelines.

Funding

This work was supported by Ministerio de Ciencia, Innovación y Universidades, la Agencia y del Fondo Europeo de Desarrollo Regional (proyecto PID2020-120267RB and PID2023-152474OB-I00 funded by *MCIU/AEI/10.13039/501100011033/FEDER, UE)* as well as by RICORS-Terav (RD24/0014/0001) funded by Instituto de Salud Carlos III and co-funded by European Union. MC-C and NL-G are recipient of the FPU fellowship from Ministerio de Ciencia, Innovación y Universidades and the Joan Oró-FI fellowship from Generalitat de Catalunya, respectively. R.L.-V. is the recipient of an ICREA Academia award.

Authors contribution

RL-V, IF-Q and designed the study, analyzed and interpreted the data and wrote the manuscript. IF-Q collected murine samples, performed the experiments, analyzed and interpreted the data and wrote the manuscript. NL-G and MC-C performed the delayed RvD1 experiments. AS-F and RL-V performed the EAE experiment. GH-M and IF-Q performed the bioinformatic analyses of the transcriptomic data. All authors read and approved the final manuscript.

CRediT authorship contribution statement

Isaac Francos-Quijorna: Writing – review & editing, Writing – original draft, Methodology, Investigation, Data curation, Conceptualization. **Néstor López-González:** Investigation. **Marc Caro-Canton:** Methodology, Investigation. **Alba Sánchez-Fernández:** Methodology, Investigation. **Gerard Hernández-Mir:** Writing – review & editing, Writing – original draft, Methodology, Investigation. **Rubèn López-Vales:** Writing – review & editing, Writing – original draft, Project administration, Methodology, Investigation, Funding acquisition, Conceptualization.

Declaration of competing interest

The authors declare the following financial interests/personal relationships which may be considered as potential competing interests:

Ruben reports financial support, article publishing charges, statistical analysis, and writing assistance were provided by Spain Ministry of Science and Innovation. Marc reports financial support and article publishing charges were provided by Spain Ministry of Science and Innovation. Nestor reports financial support and article publishing charges were provided by Government of Catalonia. Ruben reports a relationship with Autonomous University of Barcelona that includes: employment. Ruben has patent Maresins for use in the treatment of cns injuries issued to Univeristat Autònoma de Barcelona. Ruben has patent Specialized pro-resolving lipid mediators for use in the treatment of neurodegenerative diseases and/or autoimmune diseases issued to Univeristat Autònoma de Barcelona. Isaac has patent Maresins for use in the treatment of cns injuries issued to Univeristat Autònoma de Barcelona. Alba has patent Specialized pro-resolving lipid mediators for use in the treatment of neurodegenerative diseases and/or autoimmune diseases issued to Univeristat Autònoma de Barcelona. There are no additional relationships or activities to disclose If there are other authors, they declare that they have no known competing financial interests or personal relationships that could have appeared to influence the work reported in this paper.

Data availability

Data will be made available on request.

Acknowledgements

The authors thank Mónica Espejo, Jessica Jaramillo, Neus Solanas and Manuela Costa for their technical assistance.

Appendix A. Supplementary data

Supplementary data to this article can be found online at https://doi.org/10.1016/j.expneurol.2025.115226.

References

Arnold, L., Henry, A., Poron, F., Baba-Amer, Y., van Rooijen, N., Plonquet, A., Gherardi, R.K., Chazaud, B., 2007. Inflammatory monocytes recruited after skeletal muscle injury switch into antiinflammatory macrophages to support myogenesis. J. Exp. Med. 204, 1057–1069.

Bäck, M., Powell, W.S., Dahlén, S.E., Drazen, J.M., Evans, J.F., Serhan, C.N., Shimizu, T., Yokomizo, T., Rovati, G.E., 2014. Update on leukotriene, lipoxin and oxoeicosanoid receptors: IUPHAR review 7. Br. J. Pharmacol. 171, 3551–3574.

Bannenberg, G., Serhan, C.N., 2010. Specialized pro-resolving lipid mediators in the inflammatory response: an update. Biochim. Biophys. Acta 1801, 1260–1273.

Basso, D.M., Fisher, L.C., Anderson, A.J., Jakeman, L.B., McTigue, D.M., Popovich, P.G., 2006. Basso mouse scale for locomotion detects differences in recovery after spinal cord injury in five common mouse strains. J. Neurotrauma 23, 635–659.

Benjamini, Y., Hochberg, Y., 1995. Controlling the false discovery rate: a practical and powerful approach to multiple testing. J. R. Stat. Soc. B. Methodol. 57, 289–300.

Bisicchia, E., Sasso, V., Catanzaro, G., Leuti, A., Besharat, Z.M., Chiacchiarini, M., Molinari, M., Ferretti, E., Viscomi, M.T., Chiurchiù, V., 2018. Resolvin D1 halts remote Neuroinflammation and improves functional recovery after focal brain

damage via ALX/FPR2 receptor-regulated MicroRNAs. Mol. Neurobiol. 55, 6894–6905.
Buckley, C.D., Gilroy, D.W., Serhan, C.N., 2014. Proresolving lipid mediators and mechanisms in the resolution of acute inflammation. Immunity 40, 315–327.
Chiurchiù, V., Leuti, A., Dalli, J., Jacobsson, A., Battistini, L., Maccarrone, M., Serhan, C. N., 2016. Proresolving lipid mediators resolvin D1, resolvin D2, and maresin 1 are critical in modulating T cell responses. Sci. Transl. Med. 8, 353ra111.
Chiurchiù, V., Leuti, A., Saracini, S., Fontana, D., Finamore, P., Giua, R., Padovini, L., Incalzi, R.A., Maccarrone, M., 2019. Resolution of inflammation is altered in chronic heart failure and entails a dysfunctional responsiveness of T lymphocytes. FASEB J. 33, 909–916.
Coll-Miró, M., Francos-Quijorna, I., Santos-Nogueira, E., Torres-Espin, A., Bufler, P., Dinarello, C.A., López-Vales, R., 2016. Beneficial effects of IL-37 after spinal cord injury in mice. Proc. Natl. Acad. Sci. 113, 1411–1416.
De Biase, A., Knoblach, S.M., Di Giovanni, S., Fan, C., Molon, A., Hoffman, E.P., Faden, A. I., 2005. Gene expression profiling of experimental traumatic spinal cord injury as a function of distance from impact site and injury severity. Physiol. Genomics 22, 368–381.
Fiala, M., Terrando, N., Dalli, J., 2016. Specialized pro-resolving mediators from Omega-3 fatty acids improve amyloid-β phagocytosis and regulate inflammation in patients with minor cognitive impairment. J. Alzheimers Dis. 49, 1191.
Francos-Quijorna, I., Santos-Nogueira, E., Gronert, K., Sullivan, A.B., Kopp, M.A., Brommer, B., David, S., Schwab, J.M., López-Vales, R., 2017. Maresin 1 promotes inflammatory resolution, neuroprotection, and functional neurological recovery after spinal cord injury. J. Neurosci. 37, 11731–11743.
Gillespie, M., Jassal, B., Stephan, R., Milacic, M., Rothfels, K., Senff-Ribeiro, A., Griss, J., Sevilla, C., Matthews, L., Gong, C., Deng, C., Varusai, T., Ragueneau, E., Haider, Y., May, B., Shamovsky, V., Weiser, J., Brunson, T., Sanati, N., Beckman, L., Shao, X., Fabregat, A., Sidiropoulos, K., Murillo, J., Viteri, G., Cook, J., Shorser, S., Bader, G., Demir, E., Sander, C., Haw, R., Wu, G., Stein, L., Hermjakob, H., D'Eustachio, P., 2022. The reactome pathway knowledgebase 2022. Nucleic Acids Res. 50, D687–d692.
Gilligan, M.M., Gartung, A., Sulciner, M.L., Norris, P.C., Sukhatme, V.P., Bielenberg, D. R., Huang, S., Kieran, M.W., Serhan, C.N., Panigrahy, D., 2019. Aspirin-triggered proresolving mediators stimulate resolution in cancer. Proc. Natl. Acad. Sci. USA 116, 6292–6297.
Guo, Z., Hu, Q., Xu, L., Guo, Z.-N., Ou, Y., He, Y., Yin, C., Sun, X., Tang, J., Zhang, J.H., 2016. Lipoxin A4 reduces inflammation through formyl peptide receptor 2/p38 MAPK signaling pathway in subarachnoid hemorrhage rats. Stroke 47, 490–497.
Hoch, M., Rauthe, J., Cesnulevicius, K., Schultz, M., Lescheid, D., Wolkenhauer, O., Chiurchiù, V., Gupta, S., 2023. Cell-type-specific gene regulatory networks of pro-inflammatory and pro-resolving lipid mediator biosynthesis in the immune system. Int. J. Mol. Sci. 24.
Hong, S., Gronert, K., Devchand, P.R., Moussignac, R.L., Serhan, C.N., 2003. Novel docosatrienes and 17S-resolvins generated from docosahexaenoic acid in murine brain, human blood, and glial cells. Autacoids in anti-inflammation. J. Biol. Chem. 278, 14677–14687.
Irizarry, R.A., Hobbs, B., Collin, F., Beazer-Barclay, Y.D., Antonellis, K.J., Scherf, U., Speed, T.P., 2003. Exploration, normalization, and summaries of high density oligonucleotide array probe level data. Biostatistics 4, 249–264.
Kanehisa, M., 1997. A database for post-genome analysis. Trends Genet. 13, 375–376.
Klopstein, A., Santos-Nogueira, E., Francos-Quijorna, I., Redensek, A., David, S., Navarro, X., Lopez-Vales, R., 2012. Beneficial effects of alphaB-crystallin in spinal cord contusion injury. J. Neurosci. 32, 14478–14488.
Krishnamoorthy, S., Recchiuti, A., Chiang, N., Yacoubian, S., Lee, C.-H., Yang, R., Petasis, N.A., Serhan, C.N., 2010. Resolvin D1 binds human phagocytes with evidence for proresolving receptors. Proc. Natl. Acad. Sci. 107, 1660–1665.
Livak, K.J., Schmittgen, T.D., 2001. Analysis of relative gene expression data using real-time quantitative PCR and the 2−ΔΔCT method. Methods 25, 402–408.
Maderna, P., Cottell, D.C., Toivonen, T., Dufton, N., Dalli, J., Perretti, M., Godson, C., 2010. FPR2/ALX receptor expression and internalization are critical for lipoxin A4 and annexin-derived peptide-stimulated phagocytosis. FASEB J. 24, 4240–4249.
Martens, M., Ammar, A., Riutta, A., Waagmeester, A., Slenter, Denise N., Hanspers, K., Miller, A., Digles, D., Lopes, Elisson N., Ehrhart, F., Dupuis, L.J., Winckers, L.A., Coort, Susan L., Willighagen, E.L., Evelo, C.T., Pico, A.R., Kutmon, M., 2020. WikiPathways: connecting communities. Nucleic Acids Res. 49, D613–D621.
Mi, H., Muruganujan, A., Ebert, D., Huang, X., Thomas, P.D., 2019. PANTHER version 14: more genomes, a new PANTHER GO-slim and improvements in enrichment analysis tools. Nucleic Acids Res. 47, D419–d426.
Mizwicki, M.T., Liu, G., Fiala, M., Magpantay, L., Sayre, J., Siani, A., Mahanian, M., Weitzman, R., Hayden, E.Y., Rosenthal, M.J., Nemere, I., Ringman, J., Teplow, D.B., 2013. 1α,25-dihydroxyvitamin D3 and resolvin D1 retune the balance between amyloid-β phagocytosis and inflammation in Alzheimer's disease patients. J. Alzheimers Dis. 34, 155–170.
Nahrendorf, M., Swirski, F.K., Aikawa, E., Stangenberg, L., Wurdinger, T., Figueiredo, J. L., Libby, P., Weissleder, R., Pittet, M.J., 2007. The healing myocardium sequentially mobilizes two monocyte subsets with divergent and complementary functions. J. Exp. Med. 204, 3037–3047.
Norling, L.V., Dalli, J., Flower, R.J., Serhan, C.N., Perretti, M., 2012a. Resolvin D1 limits Polymorphonuclear leukocyte recruitment to inflammatory loci: receptor-dependent actions. Arterioscler. Thromb. Vasc. Biol. 32, 1970–1978.
Norling, L.V., Dalli, J., Flower, R.J., Serhan, C.N., Perretti, M., 2012b. Resolvin D1 limits polymorphonuclear leukocyte recruitment to inflammatory loci: receptor-dependent actions. Arterioscler. Thromb. Vasc. Biol. 32, 1970–1978.
Norling, L.V., Headland, S.E., Dalli, J., Arnardottir, H.H., Haworth, O., Jones, H.R., Irimia, D., Serhan, C.N., Perretti, M., 2016. Proresolving and cartilage-protective actions of resolvin D1 in inflammatory arthritis. JCI Insight 1, e85922.
Oyinbo, 2011. Secondary injury mechanisms in traumatic spinal cord injury: a nugget of this multiply cascade. Acta Neurobiol. Exp. (Wars) 71, 281–299.
Poisson, L.M., Suhail, H., Singh, J., Datta, I., Denic, A., Labuzek, K., Hoda, M.N., Shankar, A., Kumar, A., Cerghet, M., Elias, S., Mohney, R.P., Rodriguez, M., Rattan, R., Mangalam, A.K., Giri, S., 2015. Untargeted plasma metabolomics identifies endogenous metabolite with drug-like properties in chronic animal model of multiple sclerosis. J. Biol. Chem. 290, 30697–30712.
Pope, N.H., Salmon, M., Davis, J.P., Chatterjee, A., Su, G., Conte, M.S., Ailawadi, G., Upchurch Jr., G.R., 2016. D-series resolvins inhibit murine abdominal aortic aneurysm formation and increase M2 macrophage polarization. FASEB J. 30, 4192–4201.
Prüss, H., Kopp, M.A., Brommer, B., Gatzemeier, N., Laginha, I., Dirnagl, U., Schwab, J. M., 2011. Non-resolving aspects of acute inflammation after spinal cord injury (SCI): indices and resolution plateau. Brain Pathol. 21, 652–660.
Recchiuti, A., Krishnamoorthy, S., Fredman, G., Chiang, N., Serhan, C.N., 2011. MicroRNAs in resolution of acute inflammation: identification of novel resolvin D1-miRNA circuits. FASEB J. 25, 544–560.
Rogerio, A.P., Haworth, O., Croze, R., Oh, S.F., Uddin, M., Carlo, T., Pfeffer, M.A., Priluck, R., Serhan, C.N., Levy, B.D., 2012. Resolvin D1 and aspirin-triggered resolvin D1 promote resolution of allergic airways responses. J. Immunol. 189, 1983–1991.
Sanchez-Fernandez, A., Skouras, D.B., Dinarello, C.A., Lopez-Vales, R., 2019. OLT1177 (Dapansutrile), a selective NLRP3 Inflammasome inhibitor, ameliorates experimental autoimmune encephalomyelitis pathogenesis. Front. Immunol. 10, 2578.
Sanchez-Fernandez, A., Zandee, S., Mastrogiovanni, M., Charabati, M., Rubbo, H., Prat, A., Lopez-Vales, R., 2022. Administration of Maresin-1 ameliorates the physiopathology of experimental autoimmune encephalomyelitis. J. Neuroinflammation 19, 27.
Santos-Nogueira, E., López-Serrano, C., Hernández, J., Lago, N., Astudillo, A.M., Balsinde, J., Estivill-Torrús, G., de Fonseca, F.R., Chun, J., López-Vales, R., 2015. Activation of lysophosphatidic acid receptor type 1 contributes to pathophysiology of spinal cord injury. J. Neurosci. 35, 10224–10235.
Serhan, C.N., 2014. Pro-resolving lipid mediators are leads for resolution physiology. Nature 510, 92–101.
Serhan, C.N., Petasis, N.A., 2011. Resolvins and Protectins in inflammation-resolution. Chem. Rev. 111, 5922–5943.
Serhan, C.N., Chiang, N., Van Dyke, T.E., 2008. Resolving inflammation: dual anti-inflammatory and pro-resolution lipid mediators. Nat. Rev. Immunol. 8, 349–361.
Serhan, C.N., Dalli, J., Colas, R.A., Winkler, J.W., Chiang, N., 2015. Protectins and Maresins: new pro-resolving families of mediators in acute inflammation and resolution bioactive metabolome. Biochim. Biophys. Acta 1851, 397–413.
Smyth Gordon, K., 2004. Linear models and empirical Bayes methods for assessing differential expression in microarray experiments. Stat. Appl. Genet. Mol. Biol. 1.
Titos, E., Rius, B., Gonzalez-Periz, A., Lopez-Vicario, C., Moran-Salvador, E., Martinez-Clemente, M., Arroyo, V., Claria, J., 2011. Resolvin D1 and its precursor docosahexaenoic acid promote resolution of adipose tissue inflammation by eliciting macrophage polarization toward an M2-like phenotype. J. Immunol. 187, 5408–5418.
Wang, X., Zhu, M., Hjorth, E., Cortés-Toro, V., Eyjolfsdottir, H., Graff, C., Nennesmo, I., Palmblad, J., Eriksdotter, M., Sambamurti, K., Fitzgerald, J.M., Serhan, C.N., Granholm, A.C., Schultzberg, M., 2015. Resolution of inflammation is altered in Alzheimer's disease. Alzheimers Dement. 11, 40-50.e41-42.
Wickham, H., 2016. ggplot2 Elegant Graphics for Data Analysis. Springer International Publishing, Cham.
Wu, T., Hu, E., Xu, S., Chen, M., Guo, P., Dai, Z., Feng, T., Zhou, L., Tang, W., Zhan, L., Fu, X., Liu, S., Bo, X., Yu, G., 2021. clusterProfiler 4.0: a universal enrichment tool for interpreting omics data. Innovation (Camb) 2, 100141.
Yu, G., Wang, L.G., Yan, G.R., He, Q.Y., 2015. DOSE: an R/Bioconductor package for disease ontology semantic and enrichment analysis. Bioinformatics 31, 608–609.
Zhang, L., Terrando, N., Xu, Z.-Z., Bang, S., Jordt, S.-E., Maixner, W., Serhan, C.N., Ji, R.-R., 2018. Distinct analgesic actions of DHA and DHA-derived specialized pro-resolving mediators on post-operative pain after bone fracture in mice. Front. Pharmacol. 9.
Zhang, Q., Zhang, Y., Zou, M., Wu, H., Liu, C., Mi, Y., Zhu, J., Wang, Y., Jin, T., 2024. The chemically stable analogue of resolvin D1 ameliorates experimental autoimmune encephalomyelitis by mediating the resolution of inflammation. Int. Immunopharmacol. 140, 112740.
Zhu, M., Wang, X., Hjorth, E., Colas, R.A., Schroeder, L., Granholm, A.C., Serhan, C.N., Schultzberg, M., 2016. Pro-resolving lipid mediators improve neuronal survival and increase Aβ42 phagocytosis. Mol. Neurobiol. 53, 2733–2749.